Liquid Rope Coiling on a Solid Surface

M. Maleki, M. Habibi, and R. Golestanian

Institute for Advanced Studies in Basic Sciences, Zanjan 45195-159, Iran

N. M. Ribe

UMR 7579 CNRS, Institut de Physique du Globe, 4 place Jussieu, 75252 Paris cédex 05, France

Daniel Bonn

*Laboratoire de Physique Statistique, UMR 8550 CNRS, École Normale Supérieure,
24, rue Lhomond, 75231 Paris Cedex 05, France
and Van der Waals-Zeeman Institute, University of Amsterdam, Valckenierstraat 65, 1018 XE Amsterdam, The Netherlands*
(Received 17 June 2004; published 18 November 2004)

We present an experimental study of the coiling instability of a liquid "rope" falling on a solid surface. Coiling can occur in three different regimes—viscous, gravitational, or inertial—depending on the fluid viscosity and density, the fall height, and the flow rate. The competition among the different forces causes the coiling frequency first to decrease and subsequently to increase with increasing height. We also observe an oscillation between two coiling states in the gravitational-to-inertial transitional range, reflecting the multivaluedness of the dependence of coiling frequency on fall height. The data can be rescaled in a universal way, and agree very well with numerically predicted coiling frequencies.

Honey poured from a sufficient height approaches a piece of toast in the form of a rotating coil or "corkscrew" (Fig. 1). This phenomenon has been called "liquid rope coiling" [1], by analogy to the coiling of an elastic rope falling onto a surface. The latter phenomenon can be explained [2] as the bending of an elastic rod subject to gravitational and inertial forces. "Liquid ropes" are more difficult to understand because they deform simultaneously by bending, twisting, and stretching. The role of stretching [visible as the tapering of a falling stream of honey, Fig. 1(a)] is particularly important because it causes large changes in the rope's radius, the most important parameter controlling its resistance to deformation.

Liquid rope coiling has been studied extensively in the laboratory [1,3–9], and the conditions of its onset are well understood theoretically [10,11]. The first successful explanation of supercritical coiling was the Mahadevan *et al.* demonstration [12] that the dynamics of the high-frequency limit involve a balance between viscous forces and inertia. However, this is not the whole story. Recently, Ribe [13] used a numerical model for a thin viscous rope to demonstrate the existence of *three* distinct coiling regimes (viscous, gravitational, and inertial) depending on the fluid properties, the fall height, and the flow rate. These regimes are defined by the relative magnitudes of the viscous (F_V), gravitational (F_G), and inertial (F_I) forces per unit of rope length in the helical portion of the rope near the plate (the "coil"; Fig. 1(c)). Viscous coiling occurs when both gravity and inertia are negligible ($F_G, F_I \ll F_V$). Coiling in this regime is driven

entirely by the injection of the fluid, much like toothpaste squeezed from a tube. Gravitational coiling occurs when inertia is negligible and the viscous forces are balanced by gravity ($F_G \approx F_V \gg F_I$). Finally, inertial coiling occurs when gravity is negligible and viscous forces are balanced by inertia ($F_I \approx F_V \gg F_G$). To within multiplicative constants, the coiling frequencies in these three regimes are [12,13]
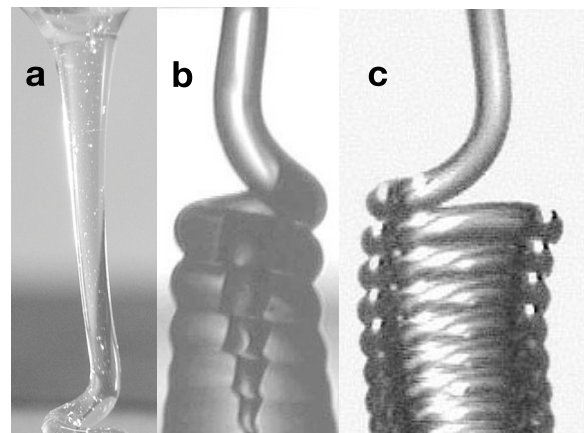

FIG. 1. Examples of liquid rope coiling. (a) Coiling of honey (viscosity $\nu = 60$ cm^2 s^{-1}) falling a distance $H = 3.4$ cm. (b) Coiling of silicone oil with $\nu = 1000$ cm^2 s^{-1}, injected from an orifice (top of image) of radius $a_0 = 0.034$ cm at a volumetric rate $Q = 0.0044$ cm^3 s^{-1}. Effective fall height $H = 0.36$ cm. (c) Coiling of silicone oil with $\nu = 125$ cm^2 s^{-1}, $a_0 = 0.1$ cm, $Q = 0.213$ cm^3 s^{-1}, and $H = 10$ cm. The radius of the portion of the rope shown is 0.04 cm.

$$\Omega_V = \frac{Q}{Ha_1^2}, \tag{1a}$$

$$\Omega_G = \left(\frac{gQ^3}{\nu a_1^8}\right)^{1/4}, \tag{1b}$$

$$\Omega_I = \left(\frac{Q^4}{\nu a_1^{10}}\right)^{1/3}, \tag{1c}$$

where Q is the volumetric flow rate, H is the fall height, ν is the kinematic viscosity, g is the gravitational acceleration, and a_1 is the radius of the rope in the coil. Surface tension changes the coiling frequencies by no more than a few percent [13], and therefore does not appear in the above expressions.

Here we report experiments covering the three regimes, with measurements of all the parameters necessary for a detailed comparison with the theory. We find that, as the fall height increases, the coiling frequency decreases and subsequently increases again, and we observe an oscillation between two coiling states with different frequencies in the gravitational-to-inertial transitional range. Finally, we show that all of the results can de rescaled in a universal way that allows us to predict the frequency of coiling of, e.g., honey on toast.

Experimental procedure.—In our experiments, silicone oil with density $\rho = 0.97$ gm cm^{-3}, surface tension coefficient $\gamma = 22$ dyne cm^{-1}, and different viscosities was injected at a constant flow rate from an orifice of radius a_0 and subsequently fell onto a metal plate. We used two different experimental setups to access the three coiling regimes. In the first setup, designed to study the transition from viscous to gravitational coiling, a syringe pump driven by a step motor was used to inject oil with viscosity $\nu = 1000$ cm^2 s^{-1} from an orifice of radius $a_0 = 0.034$ cm while the fall height H was varied. One series of experiments was performed with a flow rate $Q = 0.0038$ cm^3 s^{-1} and $H = 0.22$–1.9 cm, and another with $Q = 0.0044$ cm^3 s^{-1} and $H = 0.19$–0.92 cm. In all cases, H was measured from the orifice to the point of contact of the rope with the heap of fluid below [Fig. 1(b)]. The values of ν, Q, and H were chosen such that the rope was neither thinned significantly by gravity nor (with a few exceptions) thickened significantly by compression against the plate. The flow rate was measured from the syringe with an accuracy of 10^{-4} ml s^{-1}. A charge-coupled device camera operating at 25 frames/s was used to take movies and measure the coiling frequency by frame counting. The accuracy of the measurements of H and a_1 was about 0.2 and 0.02 mm, respectively.

In the second setup, designed to study the transition from gravitational to inertial coiling, oil with viscosity $\nu = 300$ cm^2 s^{-1} fell freely from a hole of radius $a_0 = 0.25$ cm in the bottom of a reservoir maintained at constant head. Three series of experiments were performed with $Q = 0.085$, 0.094, and 0.104 cm^3 s^{-1}, and the total

range of H was 2.0–49.4 cm. The coiling frequency was measured by filming with a high speed camera (125 to 1000 frames s^{-1}) and counting frames. The fall height, defined as above, was measured with an accuracy of 1 mm. The radius a_1 of the rope just above the coil was measured using a high-resolution digital camera. The flow rate was measured to within 1% by performing the experiment on a balance and recording the changing weight.

Frequency versus height: viscous-gravitational transition.—Figure 2(a) shows the angular coiling frequency Ω (circles) as a function of height measured using the first setup with $Q = 0.0038$ cm^3 s^{-1}. The frequency decreases strongly as a function of height for $H < 0.8$ cm, and then increases slightly thereafter. The behavior for $H < 0.8$ cm is in qualitative agreement with the scaling law (1a) for viscous coiling, which predicts $\Omega \sim H^{-1}$. In this regime, the coiling frequency is independent of viscosity and depends only on the geometry and the flow rate —even though the fluid's high viscosity is what makes coiling possible in the first place (water does not coil). The
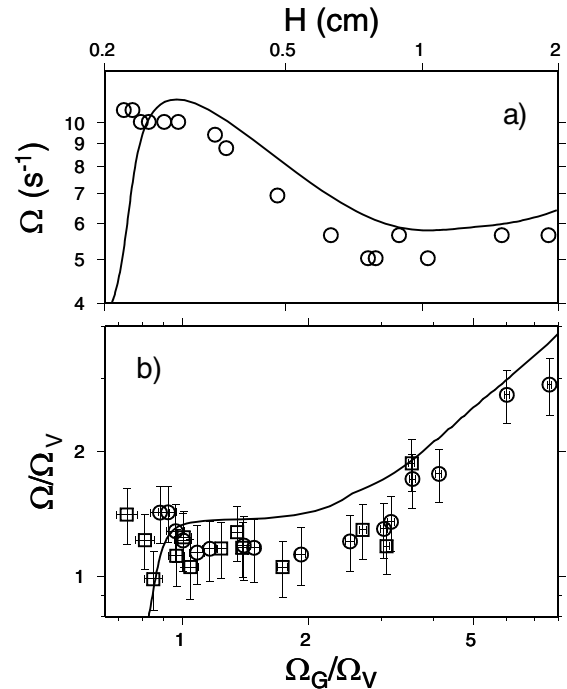

FIG. 2. Transition from viscous to gravitational coiling. (a) Open circles: angular coiling frequency measured experimentally for $\nu = 1000$ cm^2 s^{-1}, $a_0 = 0.034$ cm, and $Q = 0.0038$ cm^3 s^{-1}. Error bars on Ω and H are smaller than the diameter of the circles. Solid line: coiling frequency versus height predicted numerically for the same parameters [13]. (b) Same as (a), but rescaled using the scales Ω_V and Ω_G. Portions of the solid curve with slopes zero (left) and unity (right) correspond to viscous and gravitational coiling, respectively. Squares are for additional experiments with $Q = 0.0044$ cm^3 s^{-1}. Error bars primarily reflect uncertainty in estimation of a_1.

physical reason for this rather surprising behavior is that the velocity in the rope is determined purely kinematically by the imposed injection rate. This ceases to be the case for fall heights $H > 0.8$ cm for which the influence of gravity becomes significant, as we demonstrate below.

To analyze our experiments more precisely, we compare our data with the frequency-height curve predicted numerically for the same parameters, including surface tension for completeness [Fig. 2(a)]. The numerical predictions reproduce very well the trend of the observations, although the latter are 15%–20% too low on average, probably due to the difficulty of determining the effective value of H. At low heights the numerical model predicts a frequency that increases rapidly with height. This corresponds to coiling states in which the rope is strongly compressed against the plate, and which were discarded in the experiments.

Frequency versus height: gravitational-inertial transition.— For larger fall heights, both gravitational and inertial forces are important. Figure 3(a) shows the frequency versus height curve measured using the second setup with $Q = 0.094$ cm^3 s^{-1}. As we will see below, the low frequencies correspond to gravitational coiling, and the high frequencies to inertial coiling. These data show two remarkable features. First, and contrary to what happens in the viscous regime, the coiling frequency increases with increasing height. Second, there appears to be a discontinuous jump in the frequency at $H \approx 7$ cm.

The increase of frequency with height in the inertial regime can be understood qualitatively as follows. From (1c), $\Omega \sim a_1^{-10/3}$ in the inertial regime. The (*a priori* unknown) radius a_1 is in turn controlled by the amount of gravitational thinning that occurs in the vertical portion ("tail") of the falling rope, above the helical coil. Now the dominant forces in the coil and in the tail need not be the same: indeed, in many of our inertial coiling experiments, inertia is important in the coil but relatively minor in the tail, where gravity is balanced by viscous resistance to stretching. This implies $3\nu(AU')' \sim gA$, where 3ν is the extensional (Trouton) viscosity [14], $A = \pi a^2$ is the area of the rope's cross section, U is the axial velocity, and primes denote differentiation with respect to arclength along the tail. For strong stretching ($a_1 \ll a_0$) occurring over a distance H, the force balance implies

$$a_1 \sim (Q\nu/g)^{1/2}H^{-1}. \qquad (2)$$

Substitution of (2) into (1c) gives $\Omega \propto H^{10/3}$, roughly consistent with the slope (≈ 2.5) of the experimental data in the range $H = 9$–15 cm [Fig. 3(a)]. To do better, we need to solve the full numerical problem including all viscous, gravitational, and inertial forces. The result [Fig. 3(a), solid line] is in remarkably close agreement with the observations, with no adjustable parameters.
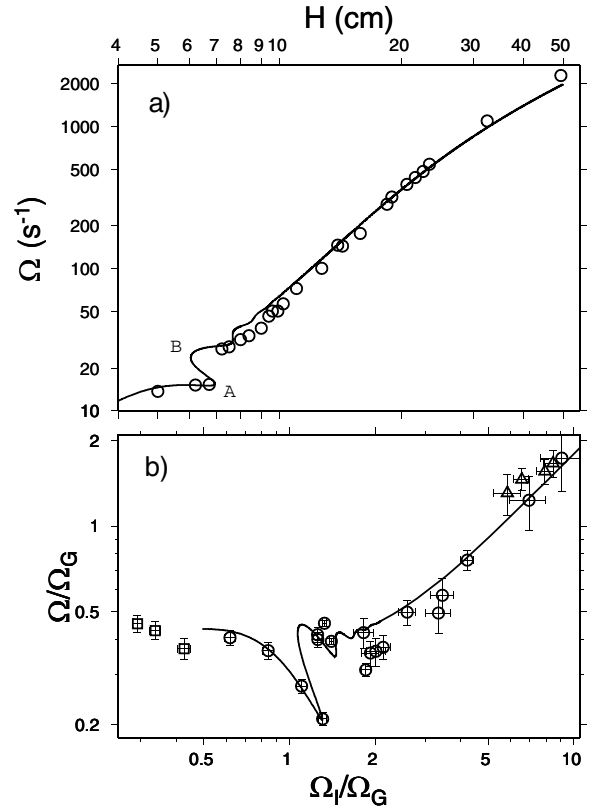

FIG. 3. Transition from gravitational to inertial coiling. (a) Circles: angular coiling frequency measured experimentally for $\nu = 300$ cm^2 s^{-1}, $a_0 = 0.25$ cm, and $Q = 0.094$ cm^3 s^{-1}. Error bars on Ω and H are smaller than the diameter of the circles. Solid line: coiling frequency versus height predicted numerically for the same parameters [13]. (b) Same as (a), but rescaled using the scales Ω_G and Ω_I. Portions of the solid curve with slopes zero and unity correspond to gravitational and inertial coiling, respectively. Results are also shown for experiments with $Q = 0.085$ cm^3 s^{-1} (squares) and 0.104 cm^3 s^{-1} (triangles).

A striking feature of the numerical frequency-height curve is its multivaluedness, which coincides perfectly with the jump in frequency observed in the experiments. These observations suggest that different coiling states with distinct frequencies may exist at the same height. To investigate this surprising behavior further, we fixed $H = 7$ cm and measured the frequency as a function of time by counting the number of video frames elapsed during each full turn (Fig. 4). We observed a clear oscillation between two frequencies that match closely the frequencies of the lower and upper branches of the numerical solutions (Fig. 4, dashed lines). The transition between the two states appears to be triggered by small changes in the height of the heap of liquid below the coils. We did not observe the state with intermediate frequency predicted by the numerics [between reference points A and B in Fig. 3(a)], which is probably unstable.
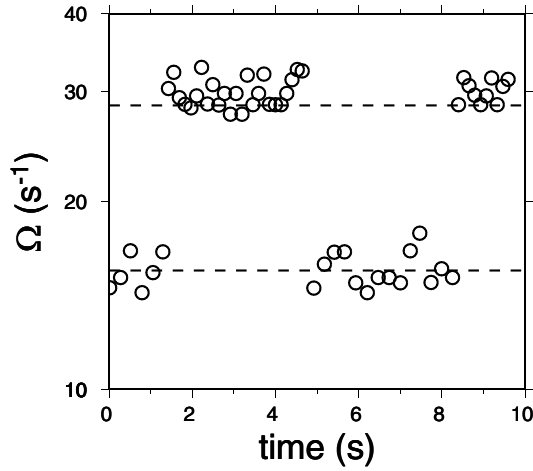
FIG. 4. Coiling frequency versus time for an experiment with $\nu = 300 \text{ cm}^2 \text{ s}^{-1}$, $a_0 = 0.25$ cm, $Q = 0.094 \text{ cm}^3 \text{ s}^{-1}$, and $H = 7.0$ cm. The dashed lines show the lowest and highest of the three coexisting frequencies predicted by the numerical solutions for the same parameters.

Universal rescaling.—Consider first the experiments performed using setup 1, which exhibit a transition from viscous to gravitational coiling. We anticipate that the control parameter for this transition will be the ratio of the characteristic frequencies Ω_G and Ω_V of the two modes, defined by (1a) and (1b). Accordingly, a log-log plot of Ω/Ω_V versus $\Omega_G/\Omega_V \equiv H(g/\nu Q)^{1/4}$ should define a universal curve, where viscous and gravitational coiling are represented by segments of slope zero and unity, respectively. To test this, we compare all of the experimental data obtained using setup 1 with the theoretically predicted universal curve in Fig. 2(b). Segments of slope zero and unity are clearly defined by the rescaled measurements, although the latter are again 15%–20% lower than the numerical predictions.

By the same reasoning, there should also exist a universal curve describing the transition from gravitational to inertial coiling as H increases. Figure 3(b) shows a log-log plot of Ω/Ω_G versus Ω_I/Ω_G for our experimental data (symbols), together with the numerical prediction (solid line). The agreement is very good, especially in the transition regime between gravitational coiling (constant Ω/Ω_G) and inertial coiling ($\Omega/\Omega_G \propto \Omega_I/\Omega_G$). Evidently the gravitational-inertial transition, such as the viscous-gravitational one, can be rescaled in such a way that the behavior is universal.

We conclude by using our results to predict the frequency of inertial coiling of honey on toast. A complete scaling law for the frequency in terms of the known experimental parameters is obtained by combining the inertial coiling law $\Omega \approx 0.18\Omega_I$ [Fig. 3(b)] with a numerical solution for a_1 valid when $a_1 \ll a_0$ [13]. This yields
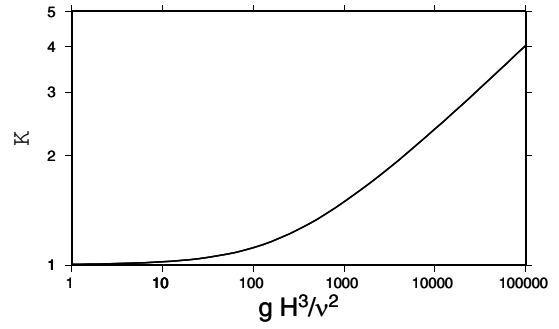

FIG. 5. Function K in (3). $K(x \to \infty) \sim (2x)^{1/4}/(\sqrt{3}\pi)$.

$$\Omega = 0.0135 g^{5/3} Q^{-1/3} \nu^{-2} \left[\frac{H}{K(gH^3/\nu^2)} \right]^{10/3}, \quad (3)$$

where the function K is shown in Fig. 5. To test this law, we measured the coiling frequency of honey ($\nu = 350 \text{ cm}^2 \text{ s}^{-1}$) falling a distance $H = 7$ cm at a rate $Q = 0.08 \text{ cm}^3 \text{ s}^{-1}$ onto a rigid surface. The measured frequency was $\Omega = 16 \text{ s}^{-1}$, while that predicted by (3) is 15.8 s^{-1}.

[1] G. Barnes and R. Woodcock, Am. J. Phys. **26**, 205 (1958).
[2] L. Mahadevan and J. B. Keller, Proc. R. Soc. London A **452**, 1679 (1996).
[3] G. Barnes and J. MacKenzie, Am. J. Phys. **27**, 112 (1959).
[4] G. I. Taylor, in *Proceedings of the 12th International Congress of Applied Mechanics* (Berlin, Springer, 1968).
[5] J. O. Cruickshank, Ph.D. thesis, Iowa State University, Ames, Iowa, 1980.
[6] J. O. Cruickshank and B. R. Munson, J. Fluid Mech. **113**, 221 (1981).
[7] R. W. Griffiths and J. S. Turner, Geophys. J. **95**, 397 (1988).
[8] H. E. Huppert, J. Fluid Mech. **173**, 557 (1986).
[9] L. Mahadevan, W. S. Ryu, and A. D. T. Samuel, Nature (London) **392**, 140 (1998).
[10] J. O. Cruickshank, J. Fluid Mech. **193**, 111 (1988).
[11] B. Tchavdarov, A. L. Yarin, and S. Radev, J. Fluid Mech. **253**, 593 (1993).
[12] L. Mahadevan, W. S. Ryu, and A. D. T. Samuel, Nature (London) **403**, 502 (2000).
[13] N. M. Ribe, Proc. R. Soc. London A **460**, 3223 (2004). Here we use slightly modified equations that include surface tension and constitutive relations that are more accurate for "thick" ropes. a_1 is calculated as the average radius of the rope over the portion of its length where the local rate of viscous dissipation due to stretching is less than 50% of the total.
[14] F. T. Trouton, Proc. R. Soc. London A **77**, 426 (1906).